

Interpretations of SUSY Searches in ATLAS with Simplified Models

Hideki Okawa, on behalf of the ATLAS Collaboration

Department of Physics and Astronomy, University of California at Irvine, Irvine, CA, USA

We present the status of interpretations of Supersymmetry (SUSY) searches in ATLAS at the Large Hadron Collider (LHC) using simplified models. Such models allow a systematic scan through the phase space in the sparticle mass plane, and in the corresponding final state kinematics. Models at various levels of simplification have been studied in ATLAS. The results can be extrapolated to more general new physics models which lead to the same event topology with similar mass hierarchies. Searches in the no-lepton channel with 1.04 fb^{-1} of data from 2011 and the same-sign dilepton channel with 35 pb^{-1} of data from 2010 are presented. No excess above the Standard Model expectation is observed, and the results are interpreted using the simplified models.

1. Introduction

ATLAS [1] at the Large Hadron Collider (LHC) [2] recorded 2.55 fb^{-1} of data by the end of August [3]. We are truly entering the TeV-scale, and starting to have a wide coverage over possible Supersymmetry (SUSY) models. In order to ensure that all the relevant phase space is covered, searches should not be over-driven by specific high energy scale SUSY models.

The simplified model approach [4][5][6] is one of the most promising model-independent strategies for new physics searches, being widely discussed both in the experimental and theoretical communities [7].

In these proceedings, the overview of the simplified model approaches used in ATLAS is presented. Brief descriptions of the ATLAS detector and dataset used in the analyses follow. Searches and simplified model interpretations in the no-lepton channel with 1.04 fb^{-1} of data from 2011 and the same-sign dilepton channel with 35 pb^{-1} of data from 2010 are described. The status of b-jet channel using simplified models is mentioned in [8].

2. Simplified Models

Simplified models are effective models built with the minimal particle content necessary to produce SUSY-like final states contributing to the channels of interest and are parametrized directly in terms of the sparticle masses. They naturally allow for reducing the dimensionality of the theoretical parameter space to two to four sparticle mass parameters and relevant branching ratios. Figure 1 shows the simplified decay chains considered in ATLAS. This approach allows to scan the whole sparticle mass plane without imposing a strict relation on the gaugino masses as are the cases in many of the high energy scale SUSY models such as mSUGRA [9][10]. Furthermore, the results can be expressed in terms of limits on cross-section times branching ratios as a function of new particle masses, separately for each event topology, or even down to each diagram, thus disentangling assumptions on the relative couplings at each vertex. The simplified model framework is a complementary approach to phenomenological Minimal Supersymmetric Standard Model (pMSSM) [11].

The results are therefore generic and can serve as an interface to theories with additional Standard Model (SM) partner particles (*e.g.* Universal Extra Dimensions, UED [12]), which make predictions in these topologies.

3. The ATLAS Detector and Data Samples

The ATLAS detector is a multipurpose particle physics apparatus with a forward-backward symmetric cylindrical geometry and near 4π coverage in solid angle¹. The inner tracking detector (ID) covers the pseudorapidity range $|\eta| < 2.5$, and consists of a silicon pixel detector, a silicon microstrip detector (SCT), and, for $|\eta| < 2.0$, a transition radiation tracker (TRT). The ID is surrounded by a thin superconducting solenoid providing a 2T

¹ATLAS uses a right-handed coordinate system with its origin at the nominal interaction point (IP) in the center of the detector and the z -axis coinciding with the axis of the beam pipe. The x -axis points from the IP to the center of the LHC ring, and the y axis points upward. Cylindrical coordinates (r, ϕ) are used in the transverse plane, ϕ being the azimuthal angle around the beam pipe. The pseudorapidity is defined in terms of the polar angle θ as $\eta = -\ln \tan(\theta/2)$.

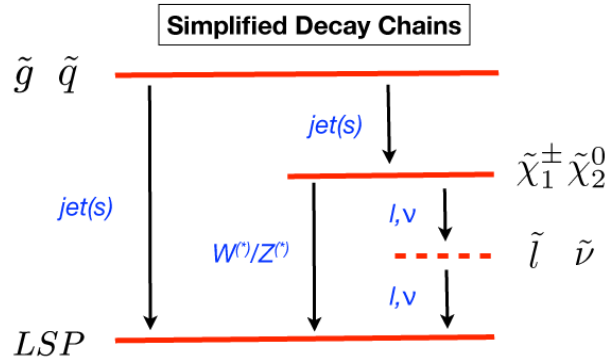


Figure 1: Simplified decay chains considered in ATLAS.

magnetic field. A high-granularity liquid-argon (LAr) sampling electromagnetic calorimeter covers the region $|\eta| < 3.2$. An iron-scintillator tile hadron calorimeter provides coverage in the central rapidity range of $|\eta| < 1.7$. The end-cap and forward regions, spanning $1.5 < |\eta| < 4.9$, are instrumented with LAr calorimetry for both electromagnetic and hadronic measurements. The muon spectrometer (MS) surrounds the calorimeters and consists of three large air-core superconducting toroids, a system of precision tracking chambers up to $|\eta| < 2.7$, and detectors for triggering in the region of $|\eta| < 2.4$.

For the no-lepton search, the data are collected in 2011 with the LHC operating at a centre-of-mass energy of 7 TeV. Application of beam, detector and data-quality requirements results in a total integrated luminosity of $1.04 \pm 0.04 \text{ fb}^{-1}$ with an estimated uncertainty of 3.7% [13]. The trigger requires events to contain a leading jet with a transverse momentum (p_T), measured at the raw electromagnetic (EM) scale, above 75 GeV and missing transverse energy (E_T^{miss}) above 45 GeV.

The data used for the same-sign dilepton analysis are recorded in 2010 at the LHC at a center-of-mass energy of 7 TeV. Similarly to the 2011 data, the application of beam, detector, and data-quality requirements results in a total integrated luminosity of 35 pb^{-1} with an estimated uncertainty of 11% [14]. The data are selected with single lepton (electron or muon) triggers. The detailed trigger requirements vary throughout the data-taking period owing to the rapidly increasing LHC luminosity and the commissioning of the trigger system, but always ensure that leptons with $p_T > 20$ GeV lie in the efficiency plateau. Monte Carlo (MC) simulation samples for background processes are generated as described in [15].

4. Object Definition

Jet candidates are reconstructed using the anti- k_t jet clustering algorithm [16][17] with a distance parameter of 0.4. The inputs to this algorithm are three-dimensional clusters of calorimeter cells [18] seeded by those with energy significantly above the measured noise. Jet momenta are constructed by performing a four-vector sum over these calorimeter clusters, treating each as an (E, \vec{p}) four-vector with zero mass. These jets are corrected for the effects of calorimeter non-compensation and inhomogeneities by using p_T and η -dependent calibration factors based on Monte Carlo (MC) simulation and validated with extensive test-beam and collision-data studies [19]. Furthermore, for 2011 data, the average additional energy due to multiple events in a single beam crossing (pile-up) is subtracted using correction constants extracted from data, and the reconstructed jet is modified such that the jet direction points to the primary vertex of the interaction instead of the geometrical center of the ATLAS detector. Only jet candidates with transverse momenta $p_T > 20$ GeV are subsequently retained.

Electron candidates are required to have $p_T > 20$ GeV, $|\eta| < 2.47$, and pass the ‘medium’ electron shower shape and track selection criteria of [20]. Muon candidates [21] are required to have $p_T > 10$ GeV (and 20 GeV for the same-sign 2-lepton analysis) and $|\eta| < 2.4$.

The measurement of the missing transverse momentum \vec{P}_T^{miss} and its magnitude, missing transverse energy E_T^{miss} is based on the transverse momenta of all electron and muon candidates, all jets which are not also electron candidates, and all calorimeter clusters with $|\eta| < 4.5$ not associated to those objects. Since tau-lepton candidates are not used in these analyses, the term “lepton” will refer only to electrons and muons.

Following the steps above, overlaps between candidate jets with $|\eta| < 2.8$ and leptons are resolved using the method of [22] as follows. First, any jet candidates lying within a distance $\Delta R = \sqrt{(\Delta\eta)^2 + (\Delta\phi)^2} = 0.2$ of

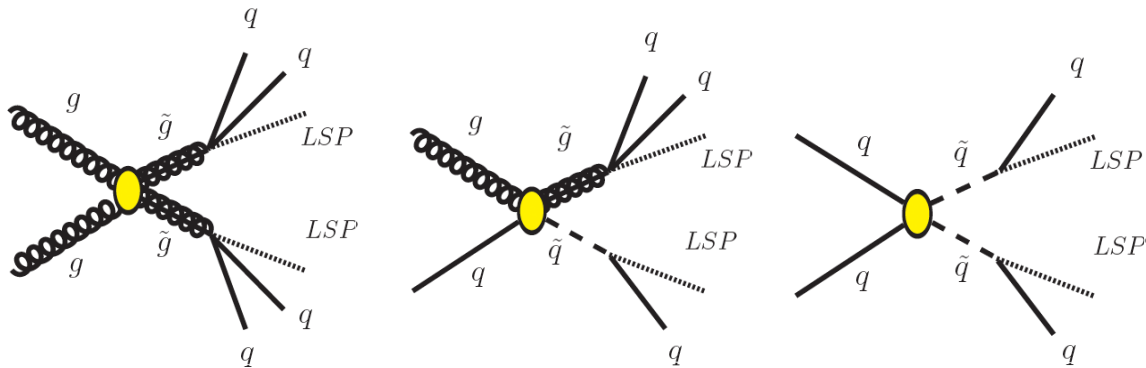


Figure 2: Simplified models considered for the no-lepton channel, where gluinos and squarks directly decay down to the LSP in the gluino-gluino (left), gluino-squark (center), and squark-squark (right) processes.

an electron are discarded, and then any electron or muon candidates remaining within a distance $\Delta R = 0.4$ of any surviving jet candidate are discarded. Next, all jet candidates with $|\eta| > 2.8$ are discarded. Finally, the remaining electron, muon and jet candidates are considered “reconstructed”, and the term “candidate” is dropped.

5. No-lepton Search

The SUSY search with all-hadronic and E_T^{miss} signature (so called “No-lepton Mode”) is considered to be one of the “golden channels.” It has the largest coverage over possible phase space of R-parity conserving pMSSM models [11].

In this search, three simplified models are considered as shown in Figure 2, where gluinos and light-flavor squarks are initially pair-produced. Direct decays to the lightest supersymmetric particles (LSPs) are considered, which are the simplest decays contributing to the no-lepton channel [5].

Five signal regions are considered to cover various regions of the gluino-squark mass plane as shown in Table I. First of all, events are discarded if electrons and muons with $p_T > 20$ GeV remain. In order to suppress detector noise and non-collision background, events are required to have the primary vertex associated with at least five tracks, and are discarded if any jets fail quality selection criteria described in [23]. Cuts on E_T^{miss} and the leading jet p_T are applied to be on the efficiency plateau of the trigger requirement. Further selections on the sub-leading jets are considered to cover event topologies from $\tilde{q}\tilde{q}$, $\tilde{g}\tilde{q}$, and $\tilde{g}\tilde{g}$ processes, where the final states consist of at least two, three, and four jets respectively. Effective mass (m_{eff}) is defined as the scalar sum of E_T^{miss} and the p_T of the two, three, four leading, or all the jets with $p_T > 40$ GeV used for each signal region. It is known to be approximately proportional to the mass of initially produced sparticles [24]. $\Delta\phi(\text{jet}, \vec{P}_T^{\text{miss}})_{\text{min}}$ and $E_T^{\text{miss}}/m_{\text{eff}}$ cuts are applied to suppress the QCD background. Two signal regions are considered for the four-jet case using different requirements on m_{eff} to cover smaller and larger mass splittings between the sparticles.

Dominant sources of background from Standard Model processes are W+jets, Z+jets, top pair, multi-jet and single top production. Non-collision background is found to be negligible.

In order to estimate the backgrounds fully or partially in data-driven ways, five control regions (CRs) are defined for each of the five signal regions (SRs), which are designed to provide uncorrelated data samples enriched with particular background sources. The observations in the CRs are used to estimate the background expectations in the SRs by using transfer factors, which are the ratios of expected event counts in the CR and SR derived independently from the CR and SR themselves. The transfer factors are obtained from MC simulations for the W+jets, Z+jets, top backgrounds, whereas for the multijet background, it is fully derived from data by smearing jets in the low E_T^{miss} events with jet response functions as is done in [25].

For the Z+jets background, irreducible contributions from $Z(\rightarrow \nu\bar{\nu})$ +jets are dominant. Two CRs are considered that are enriched with γ +jets and $Z(\rightarrow e^+e^-, \mu^+\mu^-)$ +jets, which have similar kinematics. The momentum of the photon or the dilepton system from Z is added to the \vec{P}_T^{miss} to reproduce the E_T^{miss} distribution of the $Z(\rightarrow \nu\bar{\nu})$ +jets process.

The $W(\rightarrow l\nu)$ +jets and top backgrounds are estimated from events containing one lepton and with $E_T^{\text{miss}} > 130$ GeV. Furthermore, the transverse mass $M_T = \sqrt{2p_T^l p_T^\nu (1 - \cos \Delta\phi(l, \nu))}$ is computed by assuming that the

Signal Region	≥ 2 -jet	≥ 3 -jet	≥ 4 -jet	High mass
E_T^{miss}	> 130	> 130	> 130	> 130
Leading jet p_T	> 130	> 130	> 130	> 130
Second jet p_T	> 40	> 40	> 40	> 80
Third jet p_T	–	> 40	> 40	> 80
Fourth jet p_T	–	–	> 40	> 80
$\Delta\phi(\text{jet}, \vec{P}_T^{\text{miss}})_{\text{min}}$	> 0.4	> 0.4	> 0.4	> 0.4
$E_T^{\text{miss}}/m_{\text{eff}}$	> 0.3	> 0.25	> 0.25	> 0.2
m_{eff}	> 1000	> 1000	$> 500/1000$	> 1100

Table I: Event selection for each of the five overlapping signal regions (m_{eff} , energy and momentum in GeV). Note that m_{eff} is defined with a variable number of jets, appropriate to each signal region. In the high mass selection, all jets with $p_T > 40$ GeV are used to compute the m_{eff} value used in the final cut. The $\Delta\phi(\text{jet}, \vec{P}_T^{\text{miss}})_{\text{min}}$ cut is only applied up to the third leading jet.

Process	Signal Region				
	≥ 2 -jet	≥ 3 -jet	≥ 4 -jet, $m_{\text{eff}} > 500$ GeV	≥ 4 -jet, $m_{\text{eff}} > 1000$ GeV	High mass
Z/γ +jets	$32.3 \pm 2.6 \pm 6.9$	$25.5 \pm 2.6 \pm 4.9$	$209 \pm 9 \pm 38$	$16.2 \pm 2.2 \pm 3.7$	$3.3 \pm 1.0 \pm 1.3$
W +jets	$26.4 \pm 4.0 \pm 6.7$	$22.6 \pm 3.5 \pm 5.6$	$349 \pm 30 \pm 122$	$13.0 \pm 2.2 \pm 4.7$	$2.1 \pm 0.8 \pm 1.1$
$t\bar{t}$ + single top	$3.4 \pm 1.6 \pm 1.6$	$5.9 \pm 2.0 \pm 2.2$	$425 \pm 39 \pm 84$	$4.0 \pm 1.3 \pm 2.0$	$5.7 \pm 1.8 \pm 1.9$
QCD multi-jet	$0.22 \pm 0.06 \pm 0.24$	$0.92 \pm 0.12 \pm 0.46$	$34 \pm 2 \pm 29$	$0.73 \pm 0.14 \pm 0.50$	$2.10 \pm 0.37 \pm 0.82$
Total	$62.4 \pm 4.4 \pm 9.3$	$54.9 \pm 3.9 \pm 7.1$	$1015 \pm 41 \pm 144$	$33.9 \pm 2.9 \pm 6.2$	$13.1 \pm 1.9 \pm 2.5$
Data	58	59	1118	40	18

Table II: Fitted background components in each SR, compared with the observation. In each case the first (second) quoted uncertainty is statistical (systematic). Estimates of background components are partially correlated and hence the uncertainties (statistical and systematic) on the total background estimates do not equal the quadrature sums of the uncertainties on the components.

measured E_T^{miss} provides the neutrino information, and is required to be between 30 GeV and 100 GeV to select W and top events. The events are then separated into two CRs using the b -tagging information, where jets arising from b -quarks are identified using the impact parameter and secondary vertex information. The lepton in the events is treated as a jet when computing the kinematic variables, since the dominant sources of W +jets and top backgrounds contain W 's decaying into hadronic taus and tau-neutrinos.

Finally, for the multijet background, the control region is chosen such that the cut on $\Delta\phi(\text{jet}, \vec{P}_T^{\text{miss}})_{\text{min}}$ is reversed and tightened to $\Delta\phi(\text{jet}, \vec{P}_T^{\text{miss}})_{\text{min}} < 0.2$. In such events, \vec{P}_T^{miss} is aligned with jets in the transverse plane, and E_T^{miss} originates from the mismeasurement of jets or neutrino emission from heavy flavor decays within jets. An additional and separate CR was considered to estimate the impact of the dead region in the LAr EM barrel calorimeter.

For the transfer factors derived from the MC simulation, important sources of systematic uncertainties are the jet energy scale, jet energy resolution, MC modeling uncertainties such as renormalization and factorization scale and parton distribution function (PDF) uncertainties, and uncertainty arising from the presence of pile-up. Additional uncertainties originate from photon and lepton trigger and reconstruction efficiencies, photon and lepton energy scale and resolution (for estimating the W +jets, Z +jets, and top backgrounds), b -tag/veto efficiency (for W +jets and top), photon acceptance and background (for Z +jets), and MC statistics. For the data-driven estimation of the multijet background, the main source of uncertainties for the transfer factor is the modeling of the non-Gaussian tail of the jet response function.

Table II shows the numbers of Standard Model background events expected in the signal regions, and the numbers of observed events. The m_{eff} distributions are shown in Figure 3 for each signal region. No excess is observed, and thus limits are obtained for each channel. The CL_s prescription [26] is used to set the exclusions. Figure 4 shows the combined exclusion limits for the simplified models with $m_{\text{LSP}} = 0$.

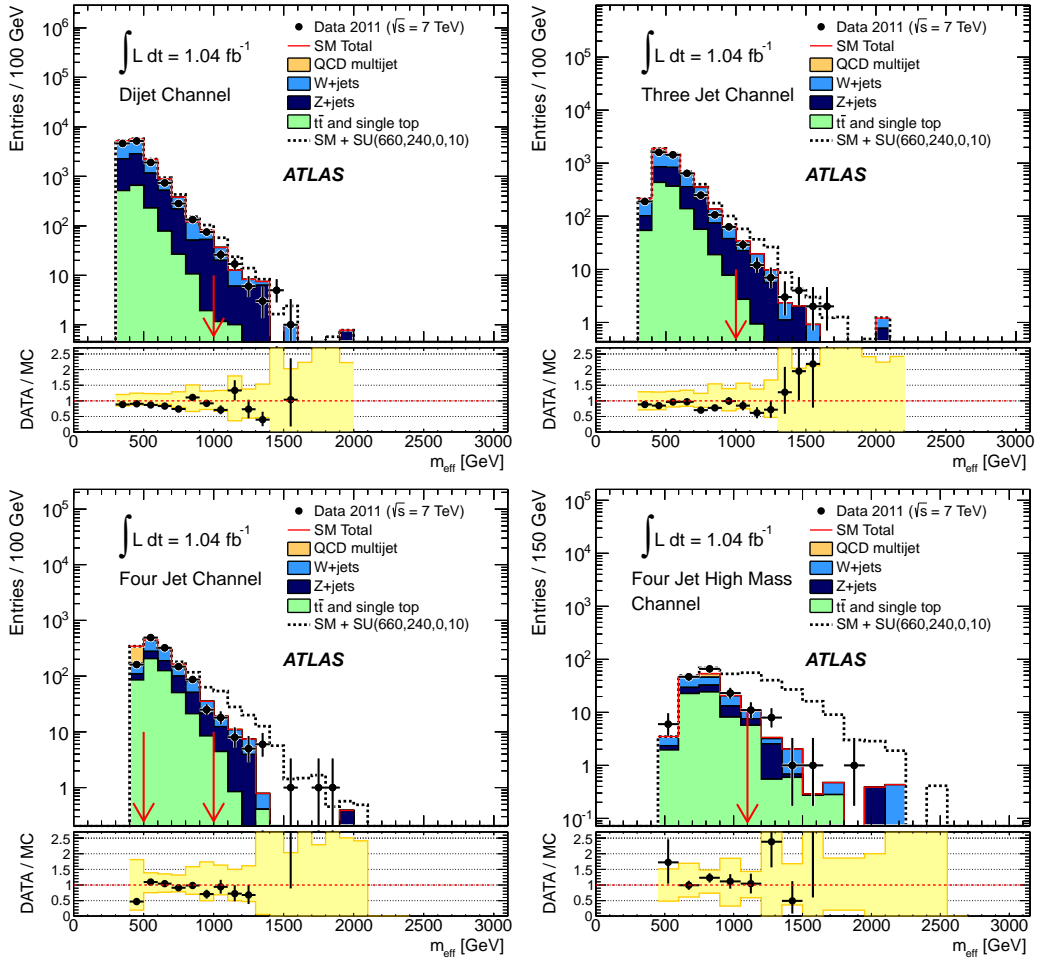


Figure 3: The m_{eff} distributions for the dijet (top left), three jet (top right), four jet (bottom left), and four jet high mass (bottom right) channels.

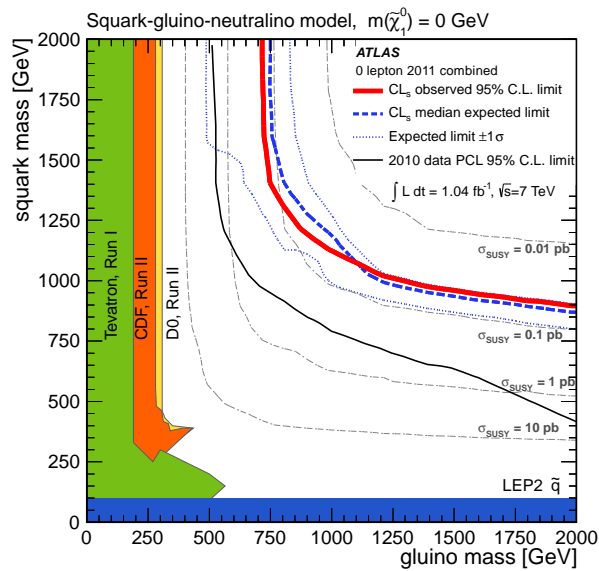


Figure 4: Combined exclusion limit for the simplified models with $m_{\text{LSP}} = 0$. The red bold line shows the observed limit at 95% CL, and the blue dashed line corresponds to the median expected 95% CL limit. The dotted blue lines show the expected 68% and 99% CL expected limits.

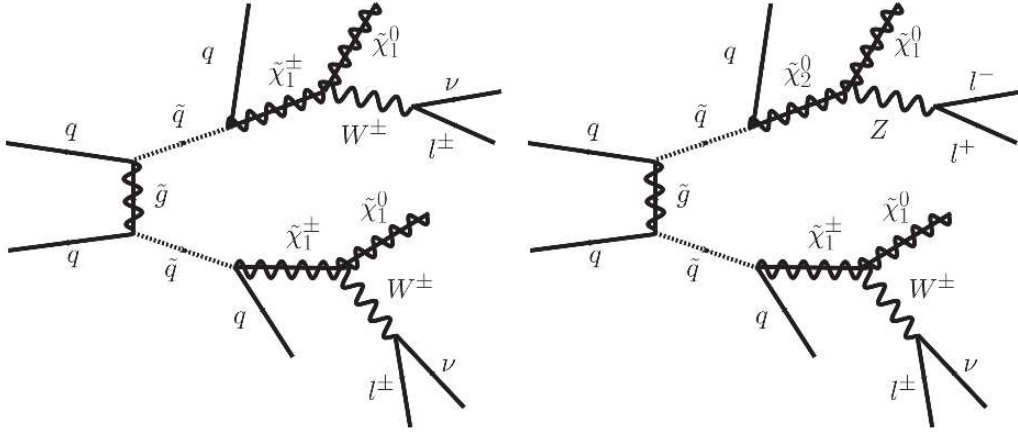


Figure 5: Simplified models with dilepton (left) and trilepton (right) final states considered for the same-sign dilepton search.

6. Same-sign Dilepton Search

A search in the same-sign dilepton channel is considered to be a clear channel for the supersymmetry search due to very low expected background from the Standard Model [27].

Here, simplified models are considered for the same-sign same-flavor squark pair production contributing to the signal region as shown in Figure 5 [28][29]. As such a process originates from the same flavor quark interactions, the contributions from the third generation squarks can be disentangled [5]. For these simplified models, there are three mass parameters: squark, weakino ($\tilde{\chi}_1^\pm, \tilde{\chi}_1^0$), and the LSP. Branching ratios are also free parameters, and the ones relevant for the diagrams are mentioned below.

$$Br(\tilde{q}\tilde{q} \rightarrow qq\ell^\pm\nu\ell^\pm\nu\tilde{\chi}_1^0\tilde{\chi}_1^0) = [Br(\tilde{q} \rightarrow q\tilde{\chi}_1^\pm)Br(\tilde{\chi}_1^\pm \rightarrow \ell^\pm\nu\tilde{\chi}_1^0)]^2 \quad (1)$$

$$Br(\tilde{q}\tilde{q} \rightarrow qq\ell\nu\ell^+\ell^-\tilde{\chi}_1^0\tilde{\chi}_1^0) = 2Br(\tilde{q} \rightarrow q\tilde{\chi}_1^\pm)Br(\tilde{q} \rightarrow q\tilde{\chi}_2^0)Br(\tilde{\chi}_1^\pm \rightarrow \ell\nu\tilde{\chi}_1^0)Br(\tilde{\chi}_2^0 \rightarrow \ell^+\ell^-\tilde{\chi}_1^0) \quad (2)$$

For this channel, events are required to have at least one reconstructed primary vertex with at least five associated tracks. Furthermore, the distance between the z coordinate of the primary vertex and that of the extrapolated muon track at the point closest to the primary vertex must be less than 10 mm to suppress cosmic background. The signal region is defined as events with exactly two identified same-sign leptons (electrons and muons) with $p_T > 20$ GeV and $E_T^{\text{miss}} > 100$ GeV.

Backgrounds from several Standard Model processes could contaminate the signal regions. The main background to the same-sign dilepton final state arises from W +jets and QCD multijet production, where one or more jets are misidentified as isolated leptons, which is referred to as “fake lepton” background. The other significant backgrounds arise from charge misidentification of an electron due to a hard bremsstrahlung process in the $t\bar{t}$ process. Contributions from Z +jets are negligible due to a high E_T^{miss} cut. Contributions from the diboson production are also estimated. The fake background is estimated in a data-driven way using the matrix method [15], and MC-based estimations are used for the other backgrounds. The cosmic background was considered and found to be negligible.

The systematic uncertainties on the data-driven fake background estimates mainly come from the parametrization of the fake rate. For the MC-driven background estimates, the jet energy scale and resolution, lepton energy scale, resolution and identification, luminosity, cross section, and parton distribution function (PDF) uncertainties are considered. More details are mentioned in [15].

No excess above the Standard Model prediction is observed as shown in Figure 6 and Table III, and upper limits on the cross-section times branching ratios for new physics based on the simplified models are obtained [29]. Classical confidence intervals in the theoretical cross section are constructed by generating ensembles of pseudo-experiments that describe the expected fluctuations of statistical and systematic uncertainties on both signal and backgrounds, following the likelihood ratio ordering prescription proposed by Feldman and Cousins [30]. The PDF uncertainty for the signals is estimated in the same way as the SM background, adopting a conservative uncertainty of 5.5%.

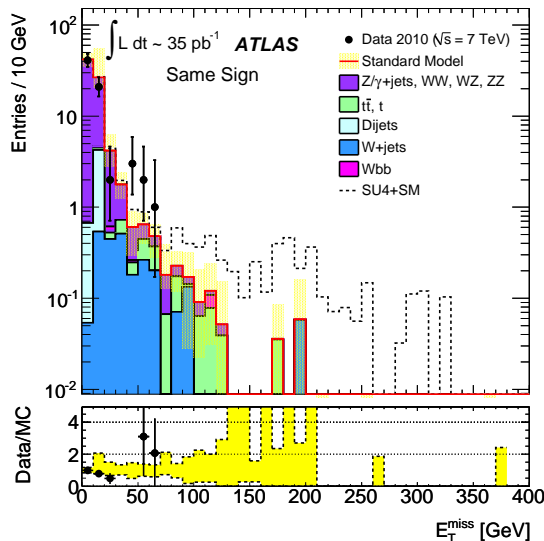

 Figure 6: Distribution of E_T^{miss} in the same-sign dilepton channel.

Table III: Summary of the background yields and observed number of events for the same sign dilepton channels.

	$e^\pm e^\pm$	$e^\pm \mu^\pm$	$\mu^\pm \mu^\pm$
Fakes	0.12 ± 0.13	0.030 ± 0.026	0.014 ± 0.010
Di-bosons	0.015 ± 0.008	0.035 ± 0.014	0.021 ± 0.006
Charge misidentification	0.019 ± 0.008	0.026 ± 0.011	-
Cosmics	-	$0_{-0}^{+1.17}$	-
Total	0.15 ± 0.13	$0.09_{-0.03}^{+1.17}$	0.04 ± 0.01
Data	0	0	0

Figure 7 shows 95% confidence level (CL) observed upper limits for each diagram as a function of $m_{\tilde{q}}$ and $m_{\tilde{\chi}_1^\pm, \tilde{\chi}_2^0}$ for the fixed LSP mass of 50 GeV. Each figure corresponds to a specific diagram, where the branching ratios are explicitly described in (1)-(2). Corresponding limit plots for the fixed LSP masses of 100 and 200 GeV, and for the diagram from a four-lepton final state are described in [29].

For each diagram, a grid of 26 signal points is produced and used for the limit setting. The upper limits are interpolated linearly from those points in three coordinates. The impact of the interpolation on the signal acceptance is found to be below a few percent and therefore does not impact the results.

7. Conclusions

No excess is found in the no-lepton channel with 1.04 fb^{-1} of data from 2011, and in the same-sign dilepton channel using 2010 data of 35 pb^{-1} . The results are interpreted with simplified models. They allow to scan wide range of sparticle mass planes, and to understand which phase space is currently covered. The simplified model approach provides model-independent interpretations and will also serve as an interface to map the results to specific models even beyond SUSY models. Interplay between different search channels is gaining more interest and importance. More simplified model results are currently under investigation.

Acknowledgments

The author would like to thank NSF and the DPF 2011 organizing committee for the partial financial support.

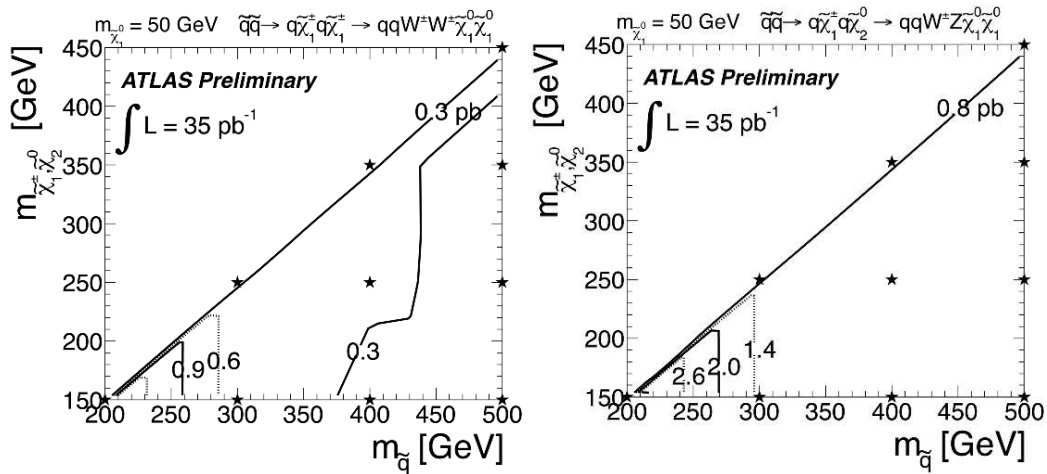


Figure 7: Observed upper limits (95% CL) on $\sigma \times \text{Br}$ in pb for the $\tilde{q}\tilde{q} \rightarrow q\tilde{\chi}_1^\pm q\tilde{\chi}_1^\pm \rightarrow qqW^\pm W^\pm \tilde{\chi}_1^0 \tilde{\chi}_1^0$ process (left) and $\tilde{q}\tilde{q} \rightarrow q\tilde{\chi}_1^\pm q\tilde{\chi}_2^0 \rightarrow qqW^\pm Z\tilde{\chi}_1^0 \tilde{\chi}_1^0$ (right) as a function of $m_{\tilde{q}}$ and $m_{\tilde{\chi}_1^\pm, \tilde{\chi}_2^0}$ for the fixed LSP mass of 50 GeV.

References

- 1 ATLAS Collaboration, JINST **3** (2008) S08003.
- 2 L. Evans and P. Bryant (editors), JINST **3** (2008) S08001.
- 3 ATLAS Collaboration, <https://twiki.cern.ch/twiki/bin/view/AtlasPublic/LuminosityPublicResults>.
- 4 N. Arkani-Hamed et al., arXiv:hep-ph/0703088 (2007).
- 5 J. Alwall et al., Phys. Rev. D **79** (2000) 015005; J. Alwall et al., Phys. Rev. D **79** (2000) 075020.
- 6 D. Alves et al., Phys. Lett. B **702** (2011) 64; D. Alves et al., arXiv:1102.5338 (2011); D. Alves et al., arXiv:1105.2838 (2011).
- 7 Signatures of New Physics at the LHC, <http://lhcnwphysics.org>.
- 8 B. Butler, in these proceedings.
- 9 A. H. Chamseddine et al., Phys. Rev. Lett. **49** (1982) 970; R. Barbieri et al., Phys. Lett. B **119** (1982) 343; L. E. Ibanez, Phys. Lett. B **118** (1982) 73; L. J. Hall et al., Phys. Rev. D **27** (1983) 2359; N. Ohta, Prog. Theor. Phys. **70** (1983) 542.
- 10 G. L. Kane et al., Phys. Rev. D **49** (1994) 6123.
- 11 C.F. Berger et al., JHEP 0902:023 (2009); J. Conley et al., Eur. Phys. J. C **71** (2011) 1697; J. Conley et al., arXiv:1103.1697 (2011); .
- 12 C. Macesanu et al., Phys. Lett. B **546** (2002) 253.
- 13 ATLAS Collaboration, ATLAS-CONF-2011-116 (2011), <http://cdsweb.cern.ch/record/1376384>.
- 14 ATLAS Collaboration, EPJC **71** (2011) 1630.
- 15 ATLAS Collaboration, EPJC **71** (2011) 1682.
- 16 M. Cacciari and G. P. Salam, JHEP **0804** (2008) 063.
- 17 M. Cacciari and G. P. Salam, Phys. Lett. B **641** (2006) 57.
- 18 ATLAS Collaboration, ATLAS-LARG-PUB-2008-002 (2008), <http://cdsweb.cern.ch/record/1099735>.
- 19 ATLAS Collaboration, ATLAS-CONF-2011-032 (2011), <http://cdsweb.cern.ch/record/1337782>.
- 20 ATLAS Collaboration, ATLAS-PHYS-PUB-2011-006 (2011), <http://cdsweb.cern.ch/record/1345327>.
- 21 ATLAS Collaboration, ATLAS-CONF-2011-063 (2011), <http://cdsweb.cern.ch/record/1345743>.
- 22 ATLAS Collaboration, arXiv:0901.0512 (2008).
- 23 ATLAS Collaboration, ATLAS-CONF-2010-038 (2010), <http://cdsweb.cern.ch/record/1277678>.
- 24 D. Tovey, EPJ Direct **4** (2002) N4.
- 25 ATLAS Collaboration, arXiv:1109.6572 (2011), submitted to Phys. Lett. B.
- 26 A. Read, Journal of Physics G: Nucl. Part. Phys. **28** (2002) 2693.
- 27 R. M. Barnett et al., Phys. Lett. B **315** (1993) 349; R. M. Barnett et al., Proc. of 1988 Summer Study on High Energy Physics in the 1990's, Snowmass, Colorado, 1988.
- 28 H. Okawa, presentation at Characterization of new physics at the LHC II, CERN, November 6, 2010.

- 29 ATLAS Collaboration, ATLAS-CONF-2011-091 (2011), <http://cdsweb.cern.ch/record/1360190>.
30 G. J. Feldman and R. D. Cousins, Phys. Rev. D **57** (1998) 3873.